

Comparative Analysis of the ZND Detonation Structure in Hydrocarbon Fuels

Calvin Colby¹, Abeetath Ghosh¹, Sai Sandeep Dammati², Alexei Poludnenko^{1,2}

¹Department of Mechanical Engineering, University of Connecticut
Storrs, CT, USA

²Department of Aerospace Engineering, Texas A&M University
College Station, TX, USA

1 Introduction

Understanding the dynamics and structure of gas-phase detonations is crucial for the design of novel detonation-based propulsion and energy conversion systems, for mitigation of fuel vapor-air explosions in industrial settings, and the development of various munitions applications. In this regard, Zeldovich-Neumann-Döring (ZND) analysis provides an important tool to determine the one-dimensional (1D) steady-state structure of a detonation in a premixed fuel/air mixture. Though it is well established that the structure and dynamics of both 1D and multi-dimensional unsteady detonations can differ significantly from their corresponding ZND solution, a steady-state ZND analysis nevertheless provides useful baseline understanding of the salient aspects of the detonation structure, including key characteristic scales such as induction and exothermic lengths. For instance, induction length obtained using the ZND analysis is frequently used to estimate the detonation cell size [1, 2], which in turn allows one to assess the detonation stability in various settings and estimate the critical channel width or detonation tube diameter for detonation propagation in simulations and experiments. Furthermore, numerical simulations often use the 1D ZND structure for detonation initialization, and the numerical resolution requirements are frequently determined based on the induction and exothermic length scales obtained from the ZND analysis.

To-date, there is no comprehensive study that systematically examines the ZND structure of detonations across a wide range of practically relevant fuel/air mixtures for different thermodynamic and chemical conditions. Here we describe a detailed database of the ZND solutions for a number of traditional fuels with particular emphasis on jet fuels. More specifically, four hydrocarbon fuels, namely ethylene (C_2H_4), single component surrogate jet fuel n-dodecane ($nC_{12}H_{26}$), JP10, and JetA2 are examined using state-of-the-art complex multistep chemical kinetics. For each fuel, we consider a range of equivalence ratios, namely $\phi = 0.5 - 1.0$, preheat temperatures, $T = 300 - 800$ K, and initial pressures, $P = 1$ and 5 bar. Several key and distinct features of the steady-state detonation properties that are unique to heavy hydrocarbons are highlighted and discussed in detail.

2 Method

The ZND profiles in this paper are generated using the CalTech Shock and Detonation Toolbox [4] in the Cantera software package [3]. The complex pyrolysis and oxidation reactions of n-dodecane,

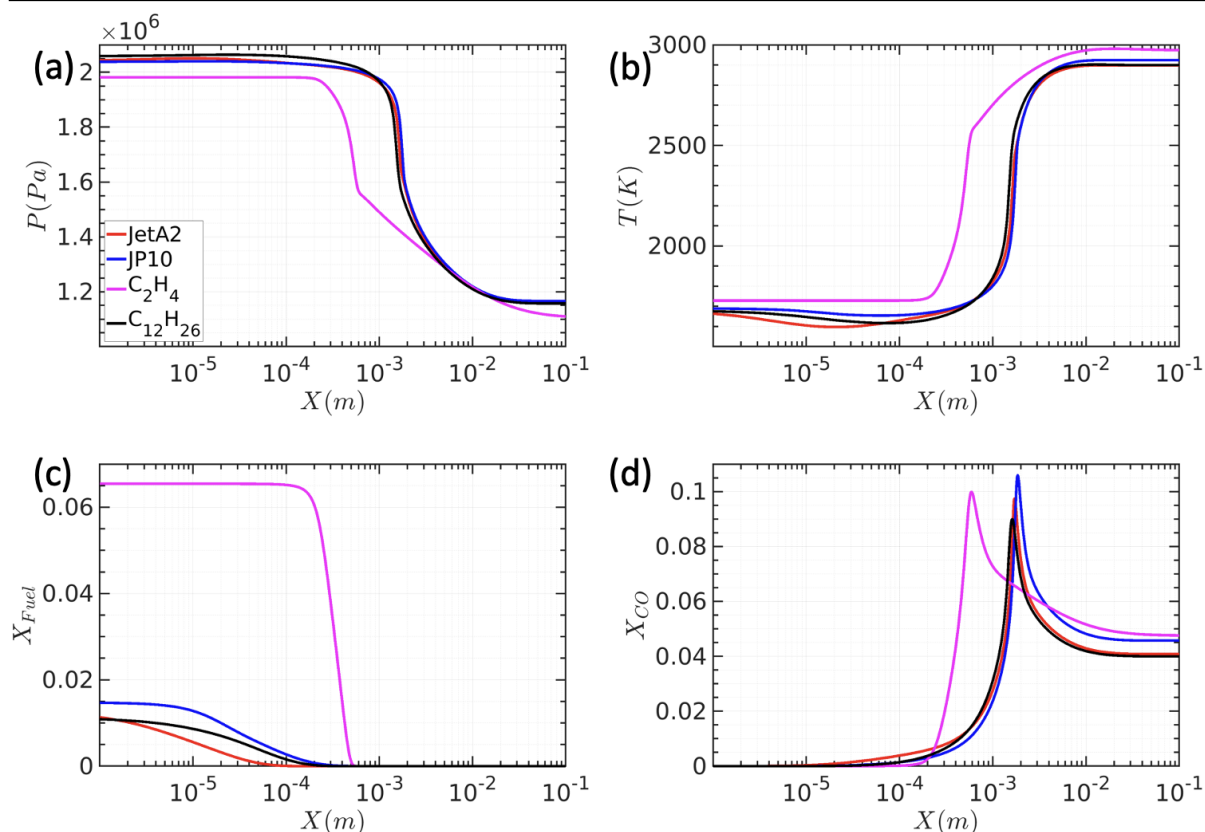


Figure 1: Distributions of pressure (a), temperature (b), fuel mole fraction (c), and CO mole fraction (d) in the ZND profiles for JetA2/air, JP10/air, C₁₂H₂₆/air, and C₂H₄/air mixtures. Preheat temperature is 500 K, initial pressure is 1 bar, and fuel equivalence ratio $\phi = 1.0$ for each fuel.

JP10, and JetA2 are modelled using reduced mechanisms from the HyChem library [5–7]. The ethylene combustion is modelled using a 30 species, 231 reactions model derived from the Foundational Fuel Chemistry Model (FFCM) series [9, 10] of reaction models. This mechanism was developed specifically for high pressure and high temperature conditions found in a detonation. The obtained ZND profiles are verified with CHEMKIN-II [8] using the same reaction mechanisms and the solutions agree well.

3 Results and Discussion

Representative ZND profiles of the four fuels examined here are shown in Fig. 1. ZND solutions for heavy hydrocarbons, namely JP10, JetA2, and n-dodecane, show very similar structure, which as can be expected differs from that in ethylene. In particular, distributions of temperature and pressure are almost identical across these heavy hydrocarbons. Previous experimental studies [2] of detonations in heavy hydrocarbons also showed that the detonation cell size and dynamics is similar for these fuels. A distinct feature that is observed across all the hydrocarbons investigated is the presence of significant amounts of the unburnt CO mass fraction as the detonation reaches chemical equilibrium (see Fig. 1d). This unique feature and its consequences will be discussed in detail below.

The key defining scales of a detonation are the induction length, Δ , and exothermic pulse width, Δ_e . In this work, we define these scales in a way similar to that in the SDToolBox. Namely Δ is the distance from the detonation front to the peak thermicity value, while Δ_e is the full width of the thermicity profile at its half maximum value, as shown in Figs. 3c and 3d, respectively. Figures 2a and 2b show

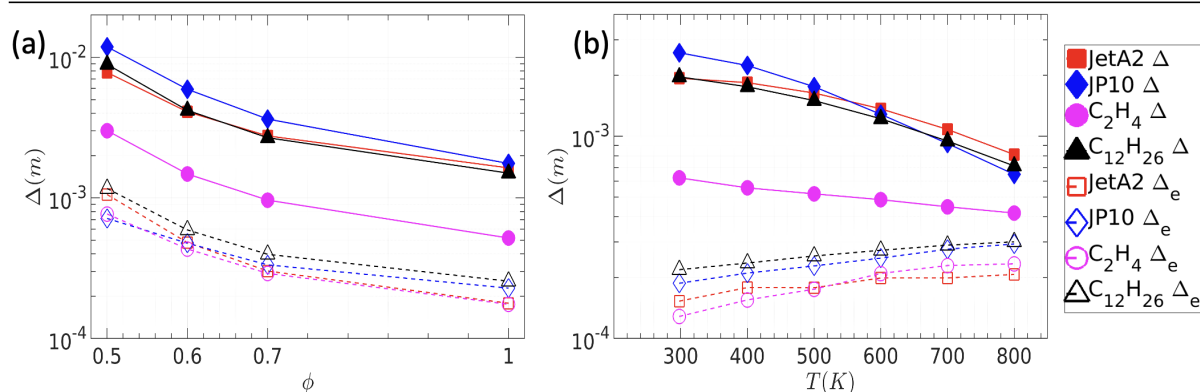


Figure 2: Induction length Δ and exothermic width Δ_e in JetA2/air, JP10/air, C_2H_4 /air, and $C_{12}H_{26}$ /air mixtures for (a) constant $T = 500$ K and for (b) constant $\phi = 1.0$. Pressure is 1 bar in both panels.

the variation of these two characteristic length scales as a function of ϕ and fuel preheat temperature, respectively, at atmospheric pressure. These length scales show similar trends for all mixtures. Δ and Δ_e tend to decrease as fuel temperature and equivalence ratio increase. In contrast to ethylene, heavier hydrocarbons have larger induction lengths, which is reflective of the higher reactivity and better detonability of ethylene. In particular, heavy hydrocarbons undergo pyrolysis, which is an endothermic process and can significantly increase the induction length/time scale. At the same time, note that the exothermic pulse widths in jet fuels are much closer to those in ethylene, with dodecane having the largest reaction zone compared to JP10 and JetA2. Finally, while the increase in ϕ decreases both Δ and Δ_e , the increase in fuel preheat has a more complex effect. In particular, higher preheat temperature lead to smaller induction lengths as can be expected, however they increase the exothermic widths for all fuels including ethylene.

3.1 Thermicity Profiles

Figure 3 shows the thermicity structure for all mixtures studied as a function of fuel preheat. Profiles are shown only for selected values of initial pressure and equivalence ratio. As expected, n-dodecane, JetA2, and JP10 mixtures contain a region with strong endothermicity immediately behind the shock due to fuel pyrolysis. The magnitude of this endothermicity tends to increase with the fuel temperature and equivalence ratio. Quantitatively, JetA2 exhibits the strongest endothermicity, with normalized thermicity reaching -32 (see Fig. 3b). Note, thermicity is normalized by its maximum value in the exothermic region. The net effect of such strong pyrolysis-driven cooling is moderated by the relatively short extent of the endothermic region of $\sim 10\mu\text{m}$, or ~ 10 ns. At high preheat temperatures, this endothermic region is followed by a characteristic bump in the thermicity profile just before the start of the exothermic zone. The size of this initial bump appears to correlate positively with the strength of endothermicity in a given fuel. For instance, note that for JetA2 the peak thermicity in this bump at $x \approx 10^{-5}$ m is 85% of the peak thermicity. As the preheat temperature decreases to 700 K, this bump weakens and starts to merge with the main thermicity peak in the reaction zone producing a thermicity profile, which monotonically increases after the endothermic region.

These effects in the induction region can be further seen in the temperature profiles in Fig. 1, where in the endothermic region the temperature initially drops behind the shock with the largest drop of ≈ 100 K exhibited by JetA2. Additionally, the jet fuel mole fractions begin to decrease immediately after the shock as the fuels get broken down. Unlike heavier hydrocarbons, ethylene does not exhibit any pronounced endothermicity or a leading thermicity bump ahead of the exothermic region (Fig. 3d). As

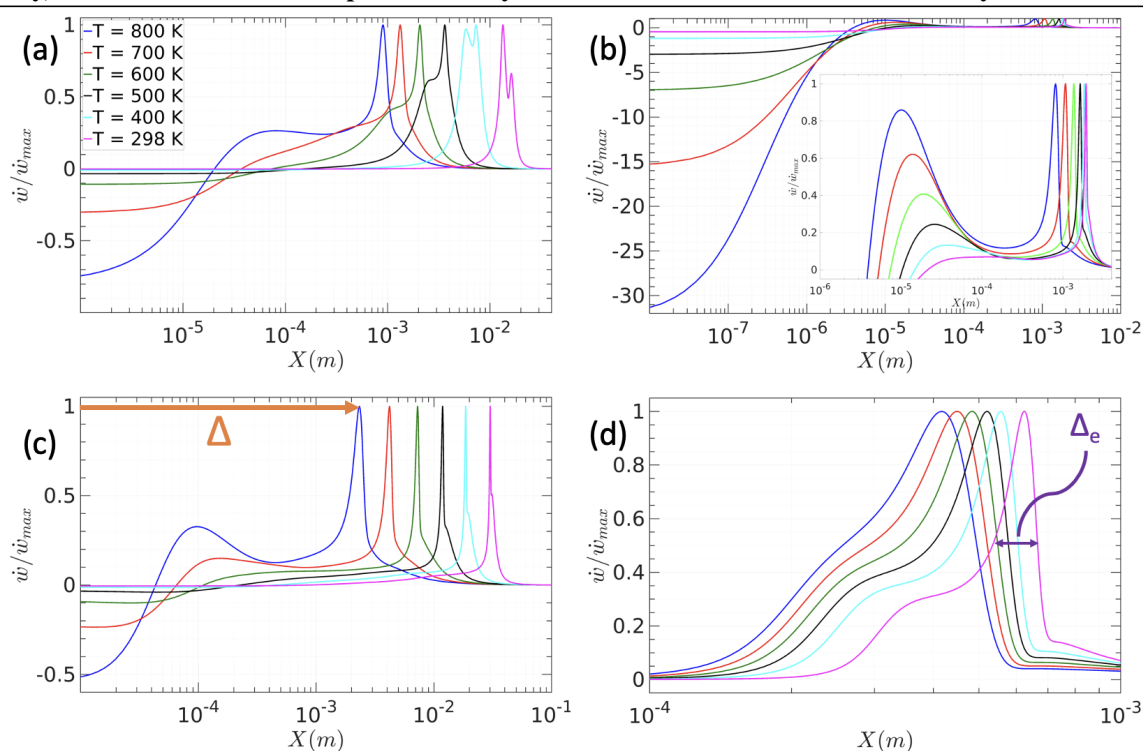


Figure 3: 1D ZND thermicity profiles for (a) $C_{12}H_{26}$ at $P = 5$ bar and $\phi = 0.5$, (b) JetA2 at $P = 1$ bar and $\phi = 1.0$, (c) JP10 at $P = 1$ bar and $\phi = 0.5$, and (d) C_2H_4 at $P = 1$ bar and $\phi = 1.0$.

a result, in ethylene, there is very little variation in the pressure, temperature, or species mole fractions in the induction zone.

We note that the presence of such complex, non-monotonic structure of thermicity in the induction zone significantly complicates the definition of the exothermic pulse width. In particular, the exothermic width value may significantly vary depending on whether the aforementioned induction zone thermicity bump reaches above or below the half-maximum thermicity cutoff, and thus whether this bump is included or not in the exothermic region. The importance of this complex endo-/exothermic induction zone structure and its effects on the detonation dynamics and stability requires further investigation.

In the reaction zone, in contrast with JetA2 and JP10, n-dodecane exhibits an interesting double-peaked structure in the shape of its thermicity profiles at low pre-heat temperatures (Fig. 1a). This feature in the thermicity profiles is more pronounced at elevated pressures and in leaner mixtures.

Finally, thermicity profiles of ethylene tend to exhibit pronounced shoulders on both sides of the reaction zone, with a more gradual shoulder on the lower temperature side associated with a two-stage heat release and a sharper one on the higher temperature one (Fig. 3d). The high-T shoulder results in a very gradual decrease in thermicity as the chemical equilibrium is being established. Its effect can be seen in the profiles of pressure and temperature (Figs. 1a and b), which show a characteristic break and subsequent gradual drop in pressure and rise in temperature toward the product state. This feature, which is associated with a suppressed CO to CO_2 conversion, is not present in heavy fuels.

3.2 CO Trapping

As the fuel is consumed, CO is produced, and it reaches its peak mole fraction roughly at the same point as the peak in thermicity. Subsequently, this CO is converted to CO_2 generating a significant portion of

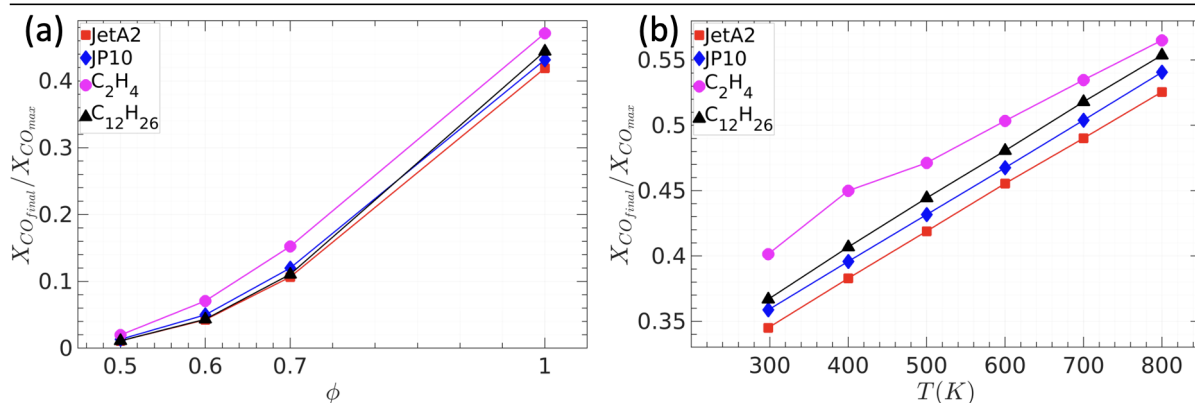


Figure 4: CO mole fraction in the product state normalized by the maximum CO mole fraction for JetA2, JP10, $C_{12}H_{26}$, and C_2H_4 mixtures at $P = 1$ bar for (a) constant $T = 500$ K and for (b) constant $\phi = 1.0$.

the overall heat release in a detonation. However, a large amount can also be left behind as reactions reach chemical equilibrium. In Fig. 4, we show the CO mole fraction in the product state normalized by the maximum CO mole fraction produced in the ZND profile for various fuel temperatures and equivalence ratios. The amount of CO trapped in products increases almost linearly with fuel preheat from $\approx 35\%$ at 300 K to $\approx 50 - 55\%$ at 800 K. The effect of equivalence ratio is comparatively stronger. For leaner mixtures at ϕ close to 0.5, the amount of CO in the products approaches zero, while at stoichiometric conditions the CO mole fraction in the products is 40 – 50% of the peak mole fraction. The primary reason for this effect is the high product temperature in richer mixtures and at higher fuel temperatures. Such high temperatures well in excess of 2500 K promote the dissociation of CO_2 shifting the balance of the $CO \rightarrow CO_2$ conversion reaction.

4 Conclusions

In this work, ZND structure of practically relevant fuel-air mixtures such as JetA2/air, JP10/air, $C_{12}H_{26}$ /air, and C_2H_4 /air is analyzed for a wide range of preheat temperatures, pressures, and equivalence ratios using SDToolbox and state-of-the-art chemical kinetics. The following key observations are made.

The thermochemical structure of all heavy hydrocarbons is very similar at the conditions examined. Such similarity could manifest in very similar dynamics and structure of multi-dimensional, unsteady detonations. The comparison of such multi-dimensional simulations will be presented in a separate work. Induction zone in jet fuels is characterized by the presence of strong endothermicity driven by fuel pyrolysis. Most notably, for JetA2, the magnitude of negative thermicity in this endothermic region can be 35 times larger than peak thermicity in the exothermic region. This results in a significant temperature drop in the induction zone reaching almost 100 K for JetA2. It is important to understand the effect of such strong endothermicity on the dynamics and, in particular, stability of both 1D and multi-dimensional detonations.

Overall ZND structure of the ethylene/air mixtures is different from that of jet fuels. In the induction zone, no pronounced endothermicity is found. At the same time, ethylene exhibits a characteristic break in thermicity at higher temperatures associated with a suppressed CO to CO_2 conversion. This results in a very gradual decrease in heat release rate and a slow temperature rise as chemical equilibrium is established. This effect can significantly extend the distance to a sonic point and thus delay the onset of thermal choking in the ethylene detonations compared to jet fuels.

Finally, we show that at higher equivalence ratios and preheat temperatures, there is a significant amount of CO trapping in the product state due to the enhancement of CO₂ dissociation at high temperatures. This effect reduces the overall heat release in a detonation front itself, which can have an effect in practical combustion systems. In particular, additional steps may need to be taken to recover energy from incomplete CO to CO₂ conversion to maximize the overall thermal efficiency.

This study will be extended to include other fuel mixtures such as H₂ and CH₄ both in air and oxygen to create a comprehensive database of ZND properties encompassing a wide range of fuels and operating conditions of practical interest. This complete database will be presented in a separate paper.

References

- [1] Westbrook CK, Urtiew PA. Chemical kinetic prediction of critical parameters in gaseous detonations. In Symposium (International) on Combustion 1982 Jan 1 (Vol. 19, No. 1, pp. 615-623). Elsevier.
- [2] Tieszen SR, Stamps DW, Westbrook CK, Pitz WJ. Gaseous hydrocarbon-air detonations. *Combustion and Flame*. 1991 Apr 1;84(3-4):376-90.
- [3] David G. Goodwin, Raymond L. Speth, Harry K. Moffat, and Bryan W. Weber. Cantera: An object-oriented software toolkit for chemical kinetics, thermodynamics, and transport processes. <https://www.cantera.org>, 2021. Version 2.5.1. doi:10.5281/zenodo.4527812
- [4] Shepherd J. E., "Shock and Detonation Toolbox," California Inst. of Technology, 2018, <https://shepherd.caltech.edu/EDL/PublicResources/sdt/>.
- [5] R. Xu, K. Wang, S. Banerjee, J. Shao, T. Parise, Y. Zhu, S. Wang, A. Movaghar, D.J. Lee, R. Zhao, X. Han, Y. Gao, T. Lu, K. Brezinsky, F.N. Egolfopoulos, D.F. Davidson, R.K. Hanson, C.T. Bowman, H. Wang, A physics-based approach to modeling real-fuel combustion chemistry - II. Reaction kinetic models of jet and rocket fuels, *Combustion and Flame* 193 (2018) 520-537.
- [6] Y. Tao, R. Xu, K. Wang, J. Shao, S.E. Johnson, A. Movaghar, X. Han, J. Park, T. Lu, K. Brezinsky, F.N. Egolfopoulos, D.F. Davidson, R.K. Hanson, C.T. Bowman, H. Wang, A physics-based approach to modeling real-fuel combustion chemistry - III. Reaction kinetic model of JP10, *Combustion and Flame* 198 (2018) 466-476.
- [7] Structure of Strongly Turbulent Premixed Flames Based on Direct Numerical Simulations and Chemical Explosive Mode Analysis, Xu, C., Poludnenko, A.Y., Zhao, X., Wang, H., Lu, T., 2019, *Combustion and Flame*, 209, 27-40
- [8] Kee, R J, Rupley, F M, Meeks, E, and Miller, J A. CHEMKIN-III: A FORTRAN chemical kinetics package for the analysis of gas-phase chemical and plasma kinetics. United States. <https://doi.org/10.2172/481621>
- [9] Tao Y, Smith GP, Wang H. Critical kinetic uncertainties in modeling hydrogen/carbon monoxide, methane, methanol, formaldehyde, and ethylene combustion. *Combustion and Flame*. 2018 Sep 1;195:18-29.
- [10] G. Smith, Y. Tao, and H. Wang, Foundational Fuel Chemistry Model Version 1.0 (FFCM-1), 2016, <http://web.stanford.edu/group/haiwanglab/FFCM1/pages/FFCM1.html>